Roles of Topological Surface States and Spin-Orbit Coupling in Catalytic Activity on Topological Insulators

Xiangting Hu,[1] Changming Zhao,[1] Xiang Huang,[1] Chao He,[1] and Hu Xu[1,2,3,*]

[1] *Department of Physics, Southern University of Science and Technology, Shenzhen 518055, People's Republic of China*

[2] *Quantum Science Center of Guangdong-Hong Kong-Macao Greater Bay Area (Guangdong), Shenzhen 518045, People's Republic of China*

[3] *Shenzhen Key Laboratory for Advanced Quantum Functional Materials and Devices, Southern University of Science and Technology, Shenzhen 518055, People's Republic of China*

(Received 6 April 2023; revised 2 July 2023; accepted 2 August 2023; published 24 August 2023)

Topological catalysis has attracted significant interest in both topological and catalytic research fields, but the underlying mechanism remains poorly understood, and the influence of topological surface states (TSSs) on catalytic activity has yet to be determined. Herein, we employ Bi_2Se_3, a prototypical topological material, to investigate the relationship between TSSs and catalytic activity. We analyze the adsorption energies of key species (e.g., H, O, and N) in heterogeneous catalysis on the $Bi_2Se_3(111)$ surface by considering both the presence and absence of TSSs. Our findings reveal that TSSs have no significant impact on adsorption energy, while spin-orbit coupling (SOC) significantly affects it. Given that topological insulators and catalytic materials containing heavy elements generally exhibit strong SOC, it is crucial to consider the role of SOC in catalytic reactions.

DOI: 10.1103/PhysRevApplied.20.024062

I. INTRODUCTION

Topological catalysis has recently emerged as a compelling interdisciplinary research area, attracting attention from the fields of condensed-matter physics, materials science, and catalytic chemistry [1–21]. Although the individual fields of topology and catalysis are well established [22–29], their intersection remains in its infancy, with many fundamental aspects yet to be elucidated [30–32]. The concept of employing topological materials as catalysts primarily stems from the presence of robust topological surface states (TSSs) [33–35], which are thought to act as an electron bath to facilitate electron transfer between reactants and catalysts. However, the underlying mechanisms governing the performance of topological materials in heterogeneous catalysis are still unclear, with insufficient evidence to confirm whether their catalytic activities originate from TSSs, trivial surface states or other material properties.

Current investigations into topological catalysis often involve comparing the catalytic performance of a topological material with that of related conventional materials, aiming to emphasize the potential role of TSSs [2–4,34,36]. For example, the catalytic performances of NbP and Pt-TiO_2 for hydrogen evolution reaction (HER) [34], $MoS_2/Bi_2Te_3/SrTiO_3$ and $MoS_2/SrTiO_3$ for HER [10], $Co_3Sn_2S_2$ and CoN or NiCo for oxygen evolution reaction (OER) [5], Bi nanosheets and Bi(110) surfaces for CO_2 reduction reaction (CO_2RR) [3], and $PdTe_2$ and Pd for ethanol oxidation reaction (EOR) [9] have been compared. However, it is challenging to determine whether the superior performance originates from TSSs of topological materials, due to the considerable variability of catalytic activity across different materials and surfaces [37]. Density-functional theory (DFT) is often utilized to study the influence of TSSs on catalytic activities, with some calculations suggesting that the adsorption energy of intermediates in catalytic processes may be affected by TSSs [18]. Nonetheless, this effect could also result from spin-orbit coupling (SOC), which is inherently introduced during calculations. Therefore, it is crucial to investigate the relationship between TSSs and the catalytic activity of topological materials while excluding other confounding factors.

Bi_2Se_3 is a key topological material with TSSs that depend on the number of layers [14,38], making it an ideal candidate for studying the relationship between catalytic activity and TSSs. By evaluating the same active site on the same surface, the influence of other factors can be minimized. In assessing catalytic activity, Sabatier's principle is widely accepted and employed [39–41], stating that the adsorption energy of intermediates on the catalyst

*xuh@sustech.edu.cn

surface is the key determinant of catalytic efficiency. Consequently, examining the effect of TSSs on adsorption energy on the Bi_2Se_3 surface is a viable approach to understanding topological catalysis.

In this work, we employ Bi_2Se_3 as a model topological material to investigate the relationship between catalytic activity and TSSs through DFT calculations. We examine the adsorption energy of H, O, and N atoms on the $Bi_2Se_3(111)$ surface with varying layer numbers, as these are critical intermediates for HER, OER, and nitrogen reduction reaction (NRR), respectively. Notably, our results show that the adsorption energy of these key species is independent of the thickness of $Bi_2Se_3(111)$, suggesting that TSSs do not affect adsorption energy. We also discover that SOC significantly impacts adsorption energy with a parabolic relationship observed between oxygen adsorption energy and SOC strength. To illustrate the generality of our conclusions, we further investigate the deposition of metal atoms and monolayers, and consider other topological materials (e.g., Bi_2Te_3). Our results reveal that TSSs have a negligible influence on the catalytic activity, while SOC should be systematically investigated in heterogeneous catalysis.

II. METHODS

We performed first-principles calculations using the projected augmented-wave method [42], as implemented in the Vienna *ab initio* simulation package [43,44]. The Perdew-Burke-Ernzerhof [45] functional with the generalized gradient approximation [46] is employed to address electron-related exchange energies. The DFT-D3 method is utilized for the van der Waals (vdW) dispersion correction [47]. Convergence criteria for force and electron relaxation are set to 0.01 eV/Å and 10^{-5} eV, respectively. A plane-wave cutoff energy is set to 400 eV. The Brillouin zone is sampled using an $11 \times 11 \times 1$ Monkhorst-Pack k mesh [48] for the (1×1) slab model. A 15-Å vacuum layer is introduced to prevent periodic interlayer interactions. The SOC effect is considered in our calculations. The adsorption energy of adsorbed species ΔE_{ad} is defined as

$$\Delta E_{ad} = \frac{E_{tot} - E_{Bi_2Se_3} - n_{atom}E_{atom}}{n_{atom}}, \quad (1)$$

where E_{tot} represents the total energy of Bi_2Se_3 with adsorbed species, $E_{Bi_2Se_3}$ is the total energy of the involved $Bi_2Se_3(111)$ slab, n_{atom} denotes the number of adsorbed atoms, and E_{atom} is the energy of a single adsorbed atom in its most stable phase.

III. RESULTS AND DISCUSSION

The top and side views of the geometrical structure of $Bi_2Se_3(111)$ are presented in Figs. 1(a) and 1(d), respectively. Given that bulk Bi_2Se_3 has a rhombohedral crystal structure with space group $R\bar{3}m$, we use hexagonal cells to calculate thin films of Bi_2Se_3. The examined $Bi_2Se_3(111)$ slab consists of a variable number (i.e., one to nine) of quintuple layers (QLs), with Bi layers sandwiched between Se layers. The bonding between two adjacent QLs is much weaker than that within QLs, which is held together by weak interlayer vdW forces. The optimized lattice constants of $Bi_2Se_3(111)$ with one–nine QLs range from 4.161 to 4.171 Å, which are in good agreement with previous theoretical and experimental values [49,50]. The band structures of different Bi_2Se_3 QLs are shown in Fig. 1 and Fig. S1 (see Supplemental Material [51]). It can be clearly seen that in the absence of SOC, the band gap gradually decreases with increasing number of layers but does not reach the point of band closure. In contrast, when SOC is introduced, the band gap closes as the film thickness reaches five QLs, consistent with previous theoretical and experimental reports that five QLs Bi_2Se_3 exhibits a nontrivial QSH phase with Dirac-core-like surface states [38,52]. Therefore, Bi_2Se_3 with one to four QLs behaves as a traditional material, while Bi_2Se_3 with five or more QLs is a topological material with TSSs.

To model surface catalysis, we considered both Se-terminated and Bi-terminated surfaces, starting with the clean Bi_2Se_3 substrate without any adsorbate. In Fig. S2(a) within the Supplemental Material [51], we present the QL-dependent energy difference of $Bi_2Se_3(111)$ with and without SOC, revealing a linear relationship. In other words, the emergence of TSSs and the interactions between layers does not change the energy difference. Next, we study oxygen adsorption on the $Bi_2Se_3(111)$ surface, as shown in Fig. 2(a). Upon adsorbing an oxygen atom on the top position of the Se atom, the calculated Se—O bond length is approximately 1.662 Å, which is consistent with the previous work [53]. Without SOC, the adsorption energy of one O atom on the one QL Bi_2Se_3 slab is calculated to be 0.425 eV. Our calculations confirm convergent adsorption energies for Bi_2Se_3 with two–nine QLs, and the corresponding ΔE_{ad} is a stable value of about 0.423 eV, as depicted in Fig. 2(a). In comparison, in the presence of SOC, ΔE_{ad} of one oxygen atom notably decreases from 0.423 to 0.275 eV, indicating a 35% reduction in the adsorption energy. This implies a strong correlation between adsorption energy and SOC strength.

Furthermore, we investigated the effect of surface oxidation on the electronic properties and TSSs in Bi_2Se_3. It is well known that the TSSs of Bi_2Se_3 arise from the band inversion of the Se-p_z orbital and the Bi-p_z orbital, which is caused by the strong SOC effect. In Fig. 2(d), we present the band structure of oxidized Bi_2Se_3 with six QLs, and additional results are provided in Fig. S3. The results indicate that the TSSs near the Fermi level remain present even after the surface oxidation. As shown in Fig. S2(b) within the Supplemental Material [51], the orbital contribution near the Γ point is not affected by the oxygen

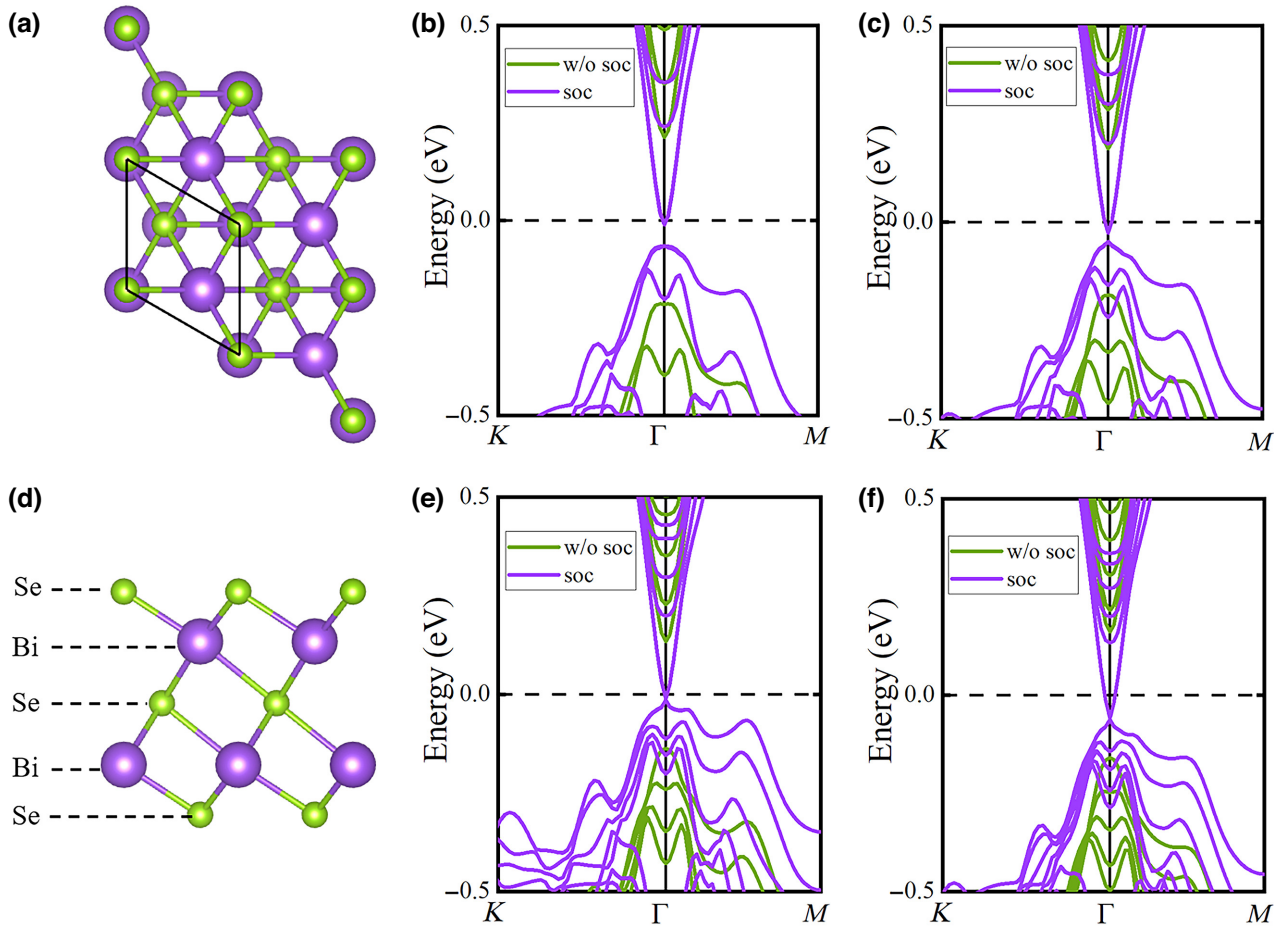

FIG. 1. (a) Top and (d) side views of $Bi_2Se_3(111)$. Only one single quintuple layer (QL) is shown and the (1×1) unit cell is marked by the black lines. Band structures of (b) three, (c) four, (e) five, and (f) six QLs without (green lines) SOC and with (purple lines) SOC. The Fermi level E_F is indicated with a dashed horizontal line.

atom, indicating that the TSSs in Bi_2Se_3 are robust against surface oxidation.

As established by the aforementioned calculations (Fig. 1) and previous theories and experiments [38,52], shows that with the inclusion of SOC, TSSs are absent in the one–four QLs of Bi_2Se_3 but present in five or more layers. From Fig. 2(a), it can be clearly seen that the plot of oxygen adsorption energy on Bi_2Se_3 for layers one–nine displays two nearly parallel lines, regardless of the presence of TSSs. Therefore, the adsorption energy of oxygen is not significantly influenced by the presence of TSSs, and the shift of ΔE_{ad} may stem from the introduction of SOC. To verify this conjecture, we plotted the curve of oxygen adsorption energy as a function of SOC strength, as shown in Fig. 3. Additional results are provided in Fig. S5 within the Supplemental Material [51]. It is apparent that the adsorption energy gradually increases with the rising strength of SOC, providing evidence that the shift in ΔE_{ad} is indeed caused by the SOC effect. This energy shift due to SOC can be explained by the nonrelativistic limit under the central force field. The steady-state Dirac equation can be expressed as follows [54,55]:

$$[c\alpha p + mc^2\beta + V(r)]\psi = E\psi, \tag{2}$$

where $V(r) = -e\phi(r)$, $p = -i\hbar\nabla$, and we can write the equation as

$$\left\{\frac{p^2}{2m} + V - \frac{p^4}{8m^3c^2} + \frac{1}{2m^2c^2}\frac{1}{r}\frac{dV}{dr}(s\cdot l) + \frac{\hbar^2}{4m^2c^2}\left(\nabla^2 V + \frac{dV}{dr}\frac{\partial}{\partial r}\right)\right\}\varphi = E'\varphi \tag{3}$$

where $(1/2m^2c^2)(1/r)(dV/dr)(s\cdot l)$ is the SOC term, which is also the source of the energy shift. This energy shift is not only related to the mass of the atom but also to the potential field surrounding the atom.

To further verify the relationship between TSSs and adsorption energy, as well as the universality of our conclusions, we performed calculations for hydrogen and nitrogen adsorption on the $Bi_2Se_3(111)$ surface. As shown

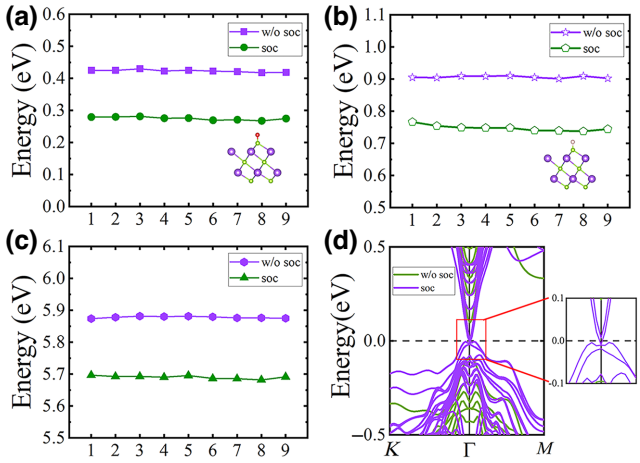

FIG. 2. The QL-dependent adsorption energies of (a) oxygen, (b) hydrogen, and (c) nitrogen on $Bi_2Se_3(111)$. (d) Band structure of oxidized six QLs $Bi_2Se_3(111)$ without (green lines) and with (purple lines) SOC. The enlarged band structure marked by the red box is shown in the right panel of (d). The Fermi level E_F is indicated with a dashed horizontal line.

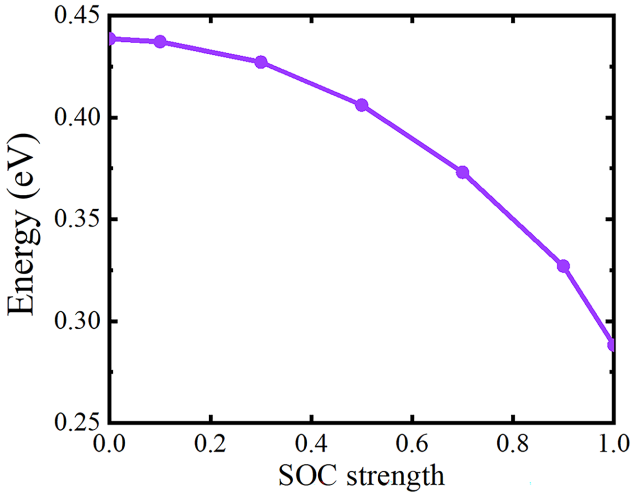

FIG. 3. Curve of oxygen adsorption energy on 5 QLs $Bi_2Se_3(111)$ as a function of SOC strength.

in Fig. 2(b), in the absence of SOC, ΔE_{ad} of H on two QLs, five QLs, and eight QLs Bi_2Se_3 were calculated to be 0.904, 0.910, and 0.909 eV, respectively. Combining the calculations for other QLs, we discovered that ΔE_{ad} of H on various $Bi_2Se_3(111)$ is around 0.908 eV, and the corresponding Gibbs free energy (ΔG_{*H}) is 1.148 eV, which is similar to the previous work on six QLs $Bi_2Se_3(111)$ [7]. When the effect of SOC is considered, ΔE_{ad} of H is reduced to around 0.748 eV, which corresponds to a decrease of approximately 0.15 eV. We found that the presence or absence of TSSs does not affect the H adsorption energy and ΔG_{*H}. Similarly, ΔE_{ad} of N was reduced from 5.881 to 5.695 eV by taking into account SOC, as shown in Fig. 2(c). These results firmly confirm that the change in ΔE_{ad} does not originate from TSSs. Notably, the influence of SOC on Bi_2Te_3 is more significant than that on Bi_2Se_3 (see Fig. 2 and Fig. S6 within the Supplemental Material [51]), indicating that the role of SOC is material dependent.

In addition to the pristine Se-terminated $Bi_2Se_3(111)$ surface, we also investigated the Bi-terminated surface to explore the adsorption behavior of oxygen, hydrogen, and nitrogen, which corresponds to the situation of surface defects common in catalytic reactions. In this configuration, the adsorbate is positioned at the top of the outermost Bi layer, and the corresponding structure is shown in Fig. S7 within the Supplemental Material [51]. By comparing Figs. 2 and 4, it can be clearly seen that ΔE_{ad} on the Bi-terminated surface is significantly enhanced compared with that on the Se-terminated surface. This finding suggests that the surface activity of Bi termination, with dangling bonds serving as active sites, is much greater than that of Se termination. Accordingly, the ΔE_{ad} values for oxygen, hydrogen, and nitrogen are about −0.878, 0.595, and 3.691 eV, respectively. When the SOC effect was introduced, ΔE_{ad} of different adsorbates increase to around −0.488, 0.878, and 4.025 eV, respectively. The corresponding band structures of Bi termination with different QLs are displayed in Figs. S8–S10 within the Supplemental Material [51]. Taking an oxidized surface as an

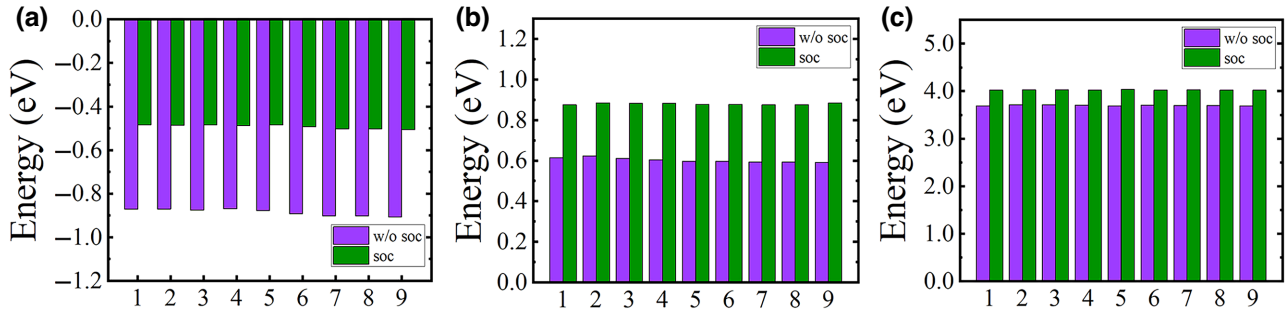

FIG. 4. The QL-dependent adsorption energies of (a) oxygen, (b) hydrogen, and (c) nitrogen in on the Bi-terminated $Bi_2Se_3(111)$ surface.

example, dangling bonds can be saturated with O atoms, and the TSSs of Bi_2Se_3 are always preserved, which are also derived from the inversion of p_z of Bi and p_z of Se. Hence, the existence of TSSs does not cause a change in ΔE_{ad}. It can be seen from Figs. 2 and 4 that SOC plays a significant role in ΔE_{ad} on Bi termination than that on Se termination, which suggests that SOC has varying effects on different materials and surfaces.

Furthermore, to exclude the roles played by TSSs, we proceeded with the investigation of the adsorption of monoatoms and monolayer (ML) of transition metals on the $Bi_2Se_3(111)$ surface. As shown in the right panel of Fig. 5(a), four different active sites were considered for the adsorption of single metal atoms: (I) above Se atoms in the second layer, (II) above Se atoms in the first layer, (III) on top of Bi atoms, and (IV) on top of Bi—Se bonds. Our results suggest that site I is energetically favorable to anchor them by binding to three Se atoms in the first layer. The calculated ΔE_{ad} of Pt, Au, and Pd on $Bi_2Se_3(111)$ are -6.224, -2.059, and -5.460 eV, respectively. Under the influence of SOC, their corresponding ΔE_{ad} values increase to -6.648, -2.658, and -5.548 eV, as shown in Figs. 5(b) and S11 within the Supplemental Material [51]. We also plot the differential charge density and calculated ΔE_{ad} of H, as shown in Fig. S12 within the Supplemental Material [51]. It is evident that the charge transfer does not change with an increase in the number of QLs. Similarly, ΔE_{ad} of H is only reduced from 0.598 to 0.547 eV under the influence of SOC [Fig. 5(c)]. Notably, the ΔE_{ad} of H shows the consistent trend as Fig. 3, that the stronger the SOC, the more impact it has on the adsorption energy. Once again, the existence of TSSs does not affect ΔE_{ad}, and the change in ΔE_{ad} is derived from the effect of SOC.

As shown in Fig. 6(a), we deposit one ML ultrathin Pt (Pd and Au) film on the $Bi_2Se_3(111)$ surface and

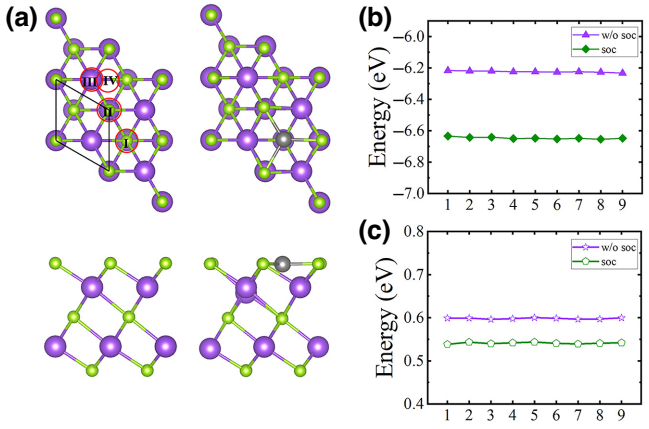

FIG. 5. (a) Top (upper left) and side (bottom left) views of possible adsorption sites (marked by red circles) for single X (X = Pt, Pd, and Au) atom on $Bi_2Se_3(111)$. The most stable adsorption configuration is shown in the right panels. The QL-dependent ΔE_{ad} of (b) Pt and (c) hydrogen.

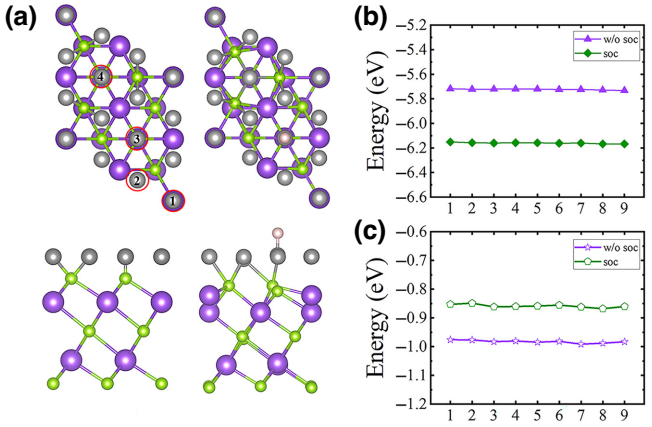

FIG. 6. (a) Top (upper left) and side (bottom left) views of possible adsorption sites (marked by red circles) for one ML Pt on $Bi_2Se_3(111)$. The most stable adsorption configuration for H adsorption is shown in the right panels. The QL-dependent ΔE_{ad} of (b) Pt and (c) hydrogen.

consider four typical H adsorption configurations. Taking into account the lattice mismatch, we use the $p(3 \times 3)$ metal layers to match $p(2 \times 2)$ $Bi_2Se_3(111)$. From Figs. 6(b) and 6(c), it can be seen that the presence of SOC enhances both ΔE_{ad} of Pt and H atoms (from -5.721 to -6.158 eV for Pt and -0.984 to -0.859 eV for H), and the presence of TSSs does not affect ΔE_{ad}, implying that TSSs have no impact on the catalytic activity of Bi_2Se_3 (the result for Pd and Au can be seen in Fig. S13 within the Supplemental Material [51]). To further support our conclusion, we present the calculated ΔG_{*H} of HER on pure metal surfaces. Our results show that the calculated ΔG_{*H} of Pt at the hydrogen coverage of 25% is about -0.124 eV, which is consistent with the generally known value of -0.09 eV [56]. Upon introducing the SOC effect, ΔG_{*H} increases to -0.025 eV, corresponding to an energy shift of about 0.1 eV. Similar trends are observed for other elements like Au and Pd in Fig. S14 within the Supplemental Material [51]. The ΔG_{*H} of Pt as a function of the strength of SOC is shown in Fig. S14 (b), which is consistent with our earlier conclusions. Additionally, Fig. S15 within the Supplemental Material [51] shows that the adsorption energy value of H on Pt decreases with the increase of SOC strength. We also find that the introduction of SOC into a non-topological system produces an energy shift. These findings indicate that SOC affects not only topological systems but also nontopological systems. Therefore, the influence of SOC should be considered in all catalysis, especially for materials with heavy elements and noncentrosymmetric materials.

IV. CONCLUSIONS

In summary, we use Bi_2Se_3 as a model material to investigate the relationship between catalytic activity and TSSs

on surfaces of topological insulators. Our results show that the presence of TSSs does not affect the adsorption energy of H, O, and N on Bi_2Se_3(111). Instead, the shift in adsorption energy is attributed to the effect of SOC, with the magnitude increasing as the strength of SOC increases. This conclusion is also applicable to Bi_2Te_3. Our results indicate that some topological insulators may coincidentally have good catalytic activities, while such properties have nothing to do with TSSs. Notably, we also find that SOC not only affects ΔE_{ad} of topological insulators but also alters ΔE_{ad} of traditional catalytic materials. Our findings clarify the issue of topological catalysis on topological insulators, and provide guidance to uncover the underlying mechanism of topological catalysis on more topological materials.

ACKNOWLEDGMENTS

This work is supported by the Science, Technology, and Innovation Commission of Shenzhen Municipality (Grant No. RCYX20200714114523069), the National Natural Science Foundation of China (Grant No. 11974160), and the Center for Computational Science and Engineering at Southern University of Science and Technology.

[1] J. Tian, S. Hong, I. Miotkowski, S. Datta, and Y. P. Chen, Observation of current-induced, long-lived persistent spin polarization in a topological insulator: A rechargeable spin battery, Sci. Adv. **3**, e1602531 (2017).

[2] J. Li, H. Ma, Q. Xie, S. Feng, S. Ullah, R. Li, J. Dong, D. Li, Y. Li, and X.-Q. Chen, Topological quantum catalyst: Dirac nodal line states and a potential electrocatalyst of hydrogen evolution in the TiSi family, Sci. China Mater. **61**, 23 (2018).

[3] H. Xie, T. Zhang, R. Xie, Z. Hou, X. Ji, Y. Pang, S. Chen, M.-M. Titirici, H. Weng, and G. Chai, Facet engineering to regulate surface states of topological crystalline insulator bismuth rhombic dodecahedrons for highly energy efficient electrochemical CO_2 reduction, Adv. Mater. **33**, 2008373 (2021).

[4] Q. Yang, G. Li, K. Manna, F. Fan, C. Felser, and Y. Sun, Topological engineering of Pt-group-metal-based chiral crystals toward high-efficiency hydrogen evolution catalysts, Adv. Mater. **32**, 1908518 (2020).

[5] G. Li, Q. Xu, W. Shi, C. Fu, L. Jiao, M. E. Kamminga, M. Yu, H. Tüysüz, N. Kumar, and V. Süß, *et al.*, Surface states in bulk single crystal of topological semimetal $Co_3Sn_2S_2$ toward water oxidation, Sci. Adv. **5**, eaaw9867 (2019).

[6] A. Politano, G. Chiarello, Z. Li, V. Fabio, L. Wang, L. Guo, X. Chen, and D. W. Boukhvalov, Toward the effective exploitation of topological phases of matter in catalysis: Chemical reactions at the surfaces of NbAs and TaAs Weyl semimetals, Adv. Funct. Mater. **28**, 1800511 (2018).

[7] L. Li, J. Zeng, W. Qin, P. Cui, and Z. Zhang, Tuning the hydrogen activation reactivity on topological insulator heterostructures, Nano Energy **58**, 40 (2019).

[8] M. Tang, H. Shen, Y. Qie, H. Xie, and Q. Sun, Edge-state-enhanced CO_2 electroreduction on topological nodal-line semimetal Cu_2Si nanoribbons, J. Phys. Chem. C **123**, 2837 (2019).

[9] Y. He, D. Yan, S. Wang, L. Shi, X. Zhang, K. Yan, and H. Luo, Topological type-II Dirac semimetal and superconductor $PdTe_2$ for ethanol electrooxidation, Energy Technol. **7**, 1900663 (2019).

[10] G. Li, J. Huang, Q. Yang, L. Zhang, Q. Mu, Y. Sun, S. Parkin, K. Chang, and C. Felser, MoS_2 on topological insulator Bi_2Te_3 thin films: Activation of the basal plane for hydrogen reduction, J. Energy Chem **62**, 516 (2021).

[11] R. M. Sattigeri, B. R. Dhori, N. N. Som, P. K. Jha, and D. Kurzydłowski, Investigation of topological and catalytic properties of gold iodide monolayer: A density functional theory study, Phys. Status Solidi RRL **16**, 2100657 (2022).

[12] X.-M. Li, Z.-Z. Lin, X.-W. Chen, and X. Chen, Selective CO_2 reduction on topological Chern magnet $TbMn_6Sn_6$, Phys. Chem. Chem. Phys. **24**, 18600 (2022).

[13] D. W. Boukhvalov, C.-N. Kuo, S. Nappini, A. Marchionni, G. D'Olimpio, J. Filippi, S. Mauri, P. Torelli, C. S. Lue, and F. Vizza, *et al.*, Efficient electrochemical water splitting with $PdSn_4$ Dirac nodal arc semimetal, ACS Catal. **11**, 7311 (2021).

[14] Q. Qu, B. Liu, J. Liang, H. Li, J. Wang, D. Pan, and I. K. Sou, Expediting hydrogen evolution through topological surface states on Bi_2Te_3, ACS Catal. **10**, 2656 (2020).

[15] X. Zhu, Y. Wang, Y. Jing, T. Heine, and Y. Li, β-$PdBi_2$ monolayer: Two-dimensional topological metal with superior catalytic activity for carbon dioxide electroreduction to formic acid, Mater. Today Adv. **8**, 100091 (2020).

[16] Q. Qu, B. Liu, H. Liu, J. Liang, J. Wang, D. Pan, and I. K. Sou, Role of topological surface states and mirror symmetry in topological crystalline insulator SnTe as an efficient electrocatalyst, Nanoscale **13**, 18160 (2021).

[17] H. Chen, W. Zhu, D. Xiao, and Z. Zhang, CO Oxidation Facilitated by Robust Surface States on Au-Covered Topological Insulators, Phys. Rev. Lett. **107**, 056804 (2011).

[18] J. Xiao, L. Kou, C.-Y. Yam, T. Frauenheim, and B. Yan, Toward rational design of catalysts supported on a topological insulator substrate, ACS Catal. **5**, 7063 (2015).

[19] S. Chen, Y.-M. Fang, J. Li, J.-J. Sun, G.-N. Chen, and H.-H. Yang, Study on the electrochemical catalytic properties of the topological insulator Bi_2Se_3, Biosens. Bioelectron. **46**, 171 (2013).

[20] Y. Chen, Y. He, H. Xu, C. Du, X. Wu, and G. Yang, Superior peroxidase mimetic activity induced by topological surface states of Weyl semimetal WTe_2, Nano Today **43**, 101421 (2022).

[21] W. Liu, X. Zhang, W. Meng, Y. Liu, X. Dai, and G. Liu, Theoretical realization of hybrid Weyl state and associated high catalytic performance for hydrogen evolution in NiSi, Iscience **25**, 103543 (2022).

[22] B. A. Bernevig and S.-C. Zhang, Quantum Spin Hall Effect, Phys. Rev. Lett. **96**, 106802 (2006).

[23] R. Yu, W. Zhang, H.-J. Zhang, S.-C. Zhang, X. Dai, and Z. Fang, Quantized anomalous Hall effect in magnetic topological insulators, Science **329**, 61 (2010).

[24] L. Fu, Topological Crystalline Insulators, Phys. Rev. Lett. **106**, 106802 (2011).

[25] L. Fu, C. L. Kane, and E. J. Mele, and Topological Insulators in Three Dimensions, Phys. Rev. Lett. **98**, 106803 (2007).
[26] J. K. Norskov and C. H. Christensen, Toward efficient hydrogen production at surfaces, Science **312**, 1322 (2006).
[27] L. Bu, S. Guo, X. Zhang, X. Shen, D. Su, G. Lu, X. Zhu, J. Yao, J. Guo, and X. Huang, Surface engineering of hierarchical platinum-cobalt nanowires for efficient electrocatalysis, Nat. Commun. **7**, 1 (2016).
[28] X. Geng, W. Sun, W. Wu, B. Chen, A. Al-Hilo, M. Benamara, H. Zhu, F. Watanabe, J. Cui, and T.-P. Chen, Pure and stable metallic phase molybdenum disulfide nanosheets for hydrogen evolution reaction, Nat. Commun. **7**, 1 (2016).
[29] T. Zhang, Y. Jiang, Z. Song, H. Huang, Y. He, Z. Fang, H. Weng, and C. Fang, Catalogue of topological electronic materials, Nature **566**, 475 (2019).
[30] G. Li and C. Felser, Heterogeneous catalysis at the surface of topological materials, Appl. Phys. Lett. **116**, 070501 (2020).
[31] R. Xie, T. Zhang, H. Weng, and G.-L. Chai, Progress, advantages, and challenges of topological material catalysts, Small Sci. **2**, 2100106 (2022).
[32] H. Luo, P. Yu, G. Li, and K. Yan, Topological quantum materials for energy conversion and storage, Nat. Rev. Phys. **4**, 611 (624).
[33] B. Bradlyn, L. Elcoro, J. Cano, M. G. Vergniory, Z. Wang, C. Felser, M. I. Aroyo, and B. A. Bernevig, Topological quantum chemistry, Nature **547**, 298 (2017).
[34] C. R. Rajamathi, U. Gupta, N. Kumar, H. Yang, Y. Sun, V. Süß, C. Shekhar, M. Schmidt, H. Blumtritt, and P. Werner, *et al.*, Weyl semimetals as hydrogen evolution catalysts, Adv. Mater. **29**, 1606202 (2017).
[35] L. Wang, Y. Yang, J. Wang, W. Liu, Y. Liu, J. Gong, G. Liu, X. Wang, Z. Cheng, and X. Zhang, Excellent catalytic performance toward the hydrogen evolution reaction in topological semimetals, EcoMat **5**, e12316 (2023).
[36] G. Li, C. Fu, W. Shi, L. Jiao, J. Wu, Q. Yang, R. Saha, M. E. Kamminga, A. K. Srivastava, and E. Liu, *et al.*, Dirac nodal arc semimetal $PtSn_4$: An ideal platform for understanding surface properties and catalysis for hydrogen evolution, Angew. Chem. **131**, 13241 (2019).
[37] C. Vogt and B. M. Weckhuysen, The concept of active site in heterogeneous catalysis, Nat. Rev. Chem. **6**, 89 (2022).
[38] Y. Zhang, K. He, C.-Z. Chang, C.-L. Song, L.-L. Wang, X. Chen, J.-F. Jia, Z. Fang, X. Dai, and W.-Y. Shan, *et al.*, Crossover of the three-dimensional topological insulator Bi_2Se_3 to the two-dimensional limit, Nat. Phys. **6**, 584 (2010).
[39] P. Sabatier, in *La catalyse en chimie organique* (C. Béranger, 1920), https://scholar.google.com/scholar_lookup?hl=en&publication_year=1913&author=P.+Sabatier&title=La+Catalyse+En+Chimie+Organique.
[40] M. Che, Nobel Prize in chemistry 1912 to Sabatier: Organic chemistry or catalysis?, Catal. Today **218**, 162 (2013).
[41] A. J. Medford, A. Vojvodic, J. S. Hummelshøj, J. Voss, F. Abild-Pedersen, F. Studt, T. Bligaard, A. Nilsson, and J. K. Nørskov, From the Sabatier principle to a predictive theory of transition-metal heterogeneous catalysis, J. Catal. **328**, 36 (2015).
[42] P. E. Blöchl, Projector augmented-wave method, Phys. Rev. B **50**, 17953 (1994).
[43] G. Kresse and J. Hafner, Ab initio molecular dynamics for liquid metals, Phys. Rev. B **47**, 558 (1993).
[44] G. Kresse and J. Furthmüller, Efficient iterative schemes for ab initio total-energy calculations using a plane-wave basis set, Phys. Rev. B **54**, 11169 (1996).
[45] J. P. Perdew, K. Burke, and M. Ernzerhof, and Generalized Gradient Approximation Made Simple, Phys. Rev. Lett. **77**, 3865 (1996).
[46] J. P. Perdew, K. Burke, and Y. Wang, Generalized gradient approximation for the exchange-correlation hole of a many-electron system, Phys. Rev. B **54**, 16533 (1996).
[47] S. Grimme, Semiempirical GGA-type density functional constructed with a long-range dispersion correction, J. Comput. Chem. **27**, 1787 (2006).
[48] H. J. Monkhorst and J. D. Pack, Special points for Brillouin-zone integrations, Phys. Rev. B **13**, 5188 (1976).
[49] H. Zhang, C.-X. Liu, X.-L. Qi, X. Dai, Z. Fang, and S.-C. Zhang, Topological insulators in Bi_2Se_3, Bi_2Te_3 and Sb_2Te_3 with a single Dirac cone on the surface, Nat. Phys. **5**, 438 (2009).
[50] T. Kato, H. Kotaka, and F. Ishii, First-principles study of surface states in topological insulators Bi_2Te_3 and Bi_2Se_3: film thickness dependence, Mol. Simul. **41**, 892 (2015).
[51] See Supplemental Material at http://link.aps.org/supplemental/10.1103/PhysRevApplied.20.024062 for band structure, adsorption energy, differential charge density, and free energy diagram.
[52] M.-X. Wang, C. Liu, J.-P. Xu, F. Yang, L. Miao, M.-Y. Yao, C. Gao, C. Shen, X. Ma, and X. Chen, *et al.*, The coexistence of superconductivity and topological order in the Bi_2Se_3 thin films, Science **336**, 52 (2012).
[53] J. Yang, B. Zheng, Z. Chen, W. Xu, R. Wang, and H. Xu, Robust topological states in Bi_2Se_3 against surface oxidation, J. Phys. Chem. C **124**, 6253 (2020).
[54] P. A. M. Dirac, The quantum theory of the electron, Proc. R. Soc. London, A **117**, 610 (1928).
[55] P. A. M. Dirac, The quantum theory of the electron. Part II, Proc. R. Soc. London, A **118**, 351 (1928).
[56] J. K. Nørskov, T. Bligaard, A. Logadottir, J. Kitchin, J. G. Chen, S. Pandelov, and U. Stimming, Trends in the exchange current for hydrogen evolution, J. Electrochem. **152**, J23 (2005).